

Flavor Symmetry and the Static Potential with Hypercubic Blocking

Anna Hasenfratz[†] and Francesco Knechtli[‡]

Physics Department, University of Colorado,
Boulder, CO 80309 USA

Abstract

We introduce a new smearing transformation, the hypercubic (HYP) fat link. The hypercubic fat link mixes gauge links within hypercubes attached to the original link only. Using quenched lattices at $\beta = 5.7$ and 6.0 we show that HYP fat links improve flavor symmetry by an order of magnitude relative to the thin link staggered action. The static potential measured on HYP smeared lattices agrees with the thin link potential at distances $r/a \geq 2$ and has greatly reduced statistical errors. These quenched results will be used in forthcoming dynamical simulations of HYP staggered fermions.

PACS number: 11.15.Ha, 12.38.Gc, 12.38.Aw

[†] e-mail: anna@eotvos.colorado.edu

[‡] e-mail: knechtli@pizero.colorado.edu

I. INTRODUCTION

Fat link actions, actions where the thin link fermionic gauge connection is replaced by a combination of extended but local gauge paths in a gauge invariant manner, have been used in a variety of quenched and dynamical simulations. Since the gauge paths of fat link actions combine only a finite number of gauge links in the local environment of the original link, fat link actions are in the same universality class as their thin link counterpart. For many physical observables fat link actions show reduced scaling violations. Staggered fat link fermions have improved flavor symmetry, both in quenched [1, 2, 3] and dynamical simulations [4, 5, 6]. Wilson-type clover fat link fermions have been studied only in quenched simulations where they show improved chiral behavior resulting in better scaling of the hadron spectrum and fewer exceptional configurations [7, 8]. Fat links have been used in overlap simulations as a starting action for evaluating Neuberger's formula [9, 10, 11]. The improved chiral properties of fat links result over an order of magnitude improvement in convergence.

It is quite intuitive to see why fat link staggered fermions show improved flavor behavior. Flavor symmetry breaking of staggered fermions is the consequence of distributing the components of the Dirac spinors to different lattice sites within a hypercube. Since each lattice site couples to different gauge fields, the different flavor and Dirac components feel different gauge environments. The original $SU(n_f) \times SU(n_f)$ symmetry is explicitly broken to a remnant $U(1)$ symmetry. Unifying the gauge fields within the hypercube would solve this problem. Smearing, while does not unify the gauge fields, can remove some of the local fluctuations thus improving flavor symmetry. The most effective smearing is one that maximally smoothes the gauge fields within the hypercube but does not extend much beyond it.

The situation is similar for Wilson fermions that break chiral symmetry explicitly. The Wilson Dirac operator is not anti-Hermitian, its eigenvalues are not constrained to the imaginary axis. The real eigenvalues spread around κ_{cr} causing spurious poles in the quenched quark propagator in the positive pion mass region [7, 8, 12, 13]. Since the real eigenvalue modes of the Dirac operator are instanton related, one can study the spread of the real eigenvalues on smooth instanton backgrounds. The real eigenmodes of the Wilson Dirac operator move farther from κ_{cr} into the positive mass region on small instantons [7]. The

Dirac operator has real modes even on configurations where the “instanton”, obtained by repeated renormalization group blocking from a large classical solution, is small with respect to the lattice spacing. These objects do not have topological interpretation, they are only dislocations, yet they are responsible for the worst spurious poles of the Dirac propagator. On ordinary Monte Carlo gauge configurations dislocations arise from large fluctuations of the plaquette. Just as dislocations distort the topological charge measurements they also distort the low lying Dirac spectrum and any physical observable related to it. Smearing removes some of the fluctuations and their corresponding spurious eigenmodes. This reduces the occurrence of exceptional configurations, improves scaling [7, 8] and makes topological charge measurement on pure gauge configurations possible [14, 15]. Again, the most effective smearing is one that maximally smoothes the gauge fields within a small, hypercube sized volume, but does not extend much beyond it.

There are observables where some fat link actions have unacceptably large scaling violations. Fattening changes the local, short distance properties of the gauge configurations. On lattices with large lattice spacing too much fattening can destroy short distance physical properties. This is most evident in the Coulomb sector of the static potential [14]. Increased levels of smearing destroy more and more of the short distance potential though it does not change the long distance string tension. The heavy-light decay constants are also very sensitive to smearing. Even low levels of smearing of the heavy fermions change the value of f_B significantly [16, 17]. Heavy fermions feel the short distance structure of the vacuum and that gets distorted by the fattening. If only the light quark action is based on fat links, this problem is avoided while the chiral properties of the light quarks are improved. These expectations are supported by preliminary results [18]. The fact that certain observables show large scaling violations with fat link actions does not mean that fat link actions are incorrect, they are just not effective in every situation.

It would be desirable to construct fat links that are local enough not to destroy short distance quantities yet smooth enough to show the desired improved chiral or flavor behavior of fat link actions. In this paper we describe a smearing transformation, hypercubic blocking, along these lines. This transformation improves flavor symmetry as much as three levels of APE blocking but mixes links from hypercubes attached to the original link only. The static potential changes only at small distances $r/a < 2$ where lattice artifacts are anyhow large. This paper deals with the definition and quenched properties of the hypercubic fat link

action. In a recent paper [6] we showed how to simulate fat link dynamical systems. We were able to simplify and modify this algorithm in such a way that dynamical simulations with the hypercubic action are possible and efficient. We used the dynamical hypercubic action to study finite temperature QCD with four flavors of staggered quarks [19].

This paper is organized as follows. In Sect. 2 we define the hypercubic blocking. The transformation has three tunable parameters. We describe how the parameters are optimized and show that as the lattice spacing decreases the transformation gets more effective, i.e. the number of smearing levels can be kept fixed and small even as one approaches the continuum limit. We show that the hypercubic action considerably improves the flavor symmetry of staggered quarks in quenched simulations. The relative improvement with respect to the standard action is about an order of magnitude and increases as the lattice spacing decreases. In Sect. 3 we present quenched results for the static potential. We show that the hypercubic action allows the determination of the Sommer scale r_0 and the string tension σ with better accuracy compared to calculations done with the thin link standard action. The distortion of the potential at small distances due to the hypercubic blocking is limited to distances $r/a < 2$ independent of the lattice spacing and rotational symmetry is also improved. In Sect. 4 we summarize our results.

II. THE HYPERCUBIC BLOCKING

A. Definition and Optimization of the Hypercubic blocking

The fat links of the hypercubic blocking (HYP) are constructed in three steps. At the final level the blocked link $V_{i,\mu}$ is constructed via projected APE blocking [20] from a set of decorated links $\tilde{V}_{i,\mu;\nu}$ as

$$V_{i,\mu} = Proj_{SU(3)}[(1 - \alpha_1)U_{i,\mu} + \frac{\alpha_1}{6} \sum_{\pm\nu \neq \mu} \tilde{V}_{i,\nu;\mu} \tilde{V}_{i+\hat{\nu},\mu;\nu} \tilde{V}_{i+\hat{\mu},\nu;\mu}^\dagger], \quad (1)$$

where $U_{i,\mu}$ is the original thin link and the index ν in $\tilde{V}_{i,\mu;\nu}$ indicates that the fat link at location i and direction μ is not decorated with staples extending in direction ν . The decorated links $\tilde{V}_{i,\mu;\nu}$ are constructed with a modified projected APE blocking from an other

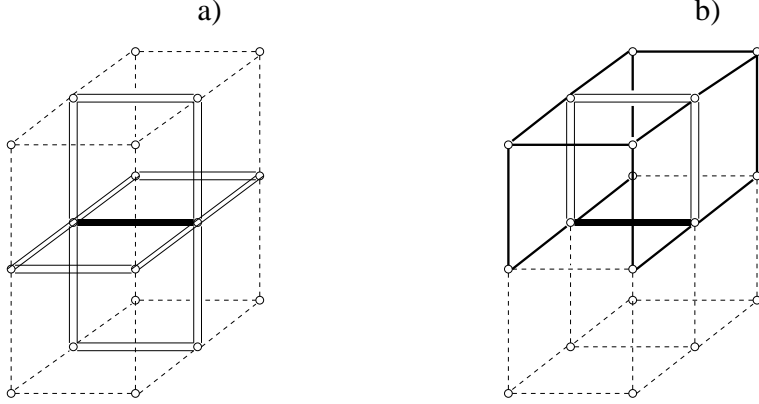


FIG. 1: Schematic representation of the hypercubic blocking in three dimensions. a) The fat link is built from the four double-lined staples. b) Each of the double-lined links is built from two staples which extend only in the hypercubes attached to the original link. An important point is that the links entering the staples are projected onto $SU(3)$.

set of decorated links, $\bar{V}_{i,\mu;\rho\nu}$ as

$$\tilde{V}_{i,\mu;\nu} = Proj_{SU(3)}[(1 - \alpha_2)U_{i,\mu} + \frac{\alpha_2}{4} \sum_{\pm\rho \neq \nu, \mu} \bar{V}_{i,\rho;\nu\mu} \bar{V}_{i+\hat{\rho},\mu;\rho\nu} \bar{V}_{i+\hat{\mu},\rho;\nu\mu}^\dagger], \quad (2)$$

where the indices $\rho\nu$ indicate that the fat link $\bar{V}_{i,\mu;\rho\nu}$ in direction μ is not decorated with staples extending in the ρ or ν directions. The decorated links $\bar{V}_{i,\mu;\rho\nu}$ are constructed from the original thin links with a modified projected APE blocking step

$$\bar{V}_{i,\mu;\nu\rho} = Proj_{SU(3)}[(1 - \alpha_3)U_{i,\mu} + \frac{\alpha_3}{2} \sum_{\pm\eta \neq \rho, \nu, \mu} U_{i,\eta} U_{i+\hat{\eta},\mu} U_{i+\hat{\mu},\eta}^\dagger]. \quad (3)$$

Here only the two staples orthogonal to μ, ν and ρ are used. With the construction eqs. (1)-(3) the fat link $V_{i,\mu}$ mixes thin links only from hypercubes attached to the original link. The hypercubic blocking is schematically represented in figure 1. The parameters α_1, α_2 and α_3 can be optimized to achieve the smoothest blocked link configuration. The construction eqs. (1)-(3) can be iterated.

We could use a physical quantity like the level of flavor symmetry restoration to optimize the parameters of the blocking, but in a three dimensional parameter space that approach is very computer intensive. Instead we have decided to look at the underlying reason of flavor and chiral symmetry violation. As we explained in the introduction, both the staggered fermions' flavor symmetry violation and Wilson fermions' exceptional configurations can be understood as fluctuations in the local plaquette. It is not the average, not even the

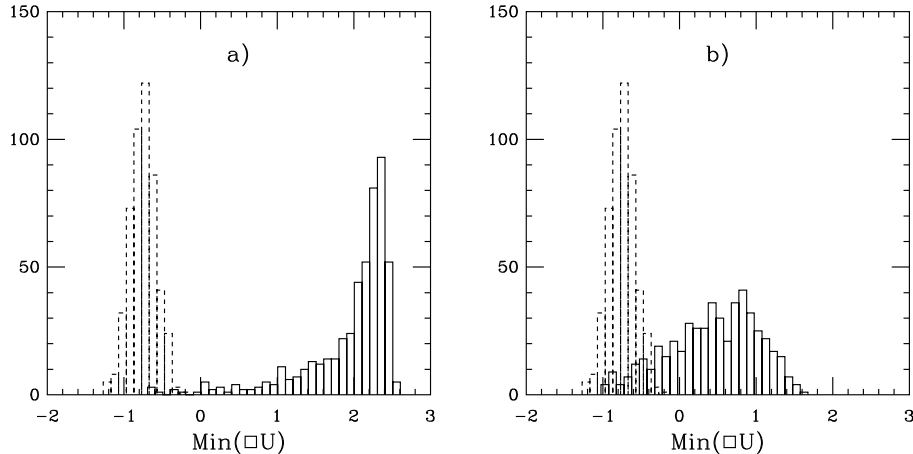


FIG. 2: a) The histogram of the smallest plaquette distribution on a set of 4^4 $\beta = 5.7$ configurations (dashed lines) and after hypercubic blocking (solid lines) on the same configurations. b) Same as a) but the solid lines correspond to one level APE smearing with $\alpha = 0.7$.

average fluctuation of the plaquette that causes the problems but the few largest plaquette fluctuations that create dislocations. To minimize the largest fluctuations we have to maximize the smallest plaquettes of the system. We do this by considering the distribution of the smallest plaquette in a finite, fixed volume lattice. The optimized hypercubic blocking parameters will give the largest expectation value for the smallest plaquette in this finite volume ensemble. We have optimized the α parameters using a set of 500 4^4 lattices created at $\beta = 5.7$ with the Wilson plaquette action.

Figure 2/a shows the histogram of the smallest plaquette on each of the 500 original configurations (dashed lines) and after hypercubic blocking (solid lines) with parameters

$$\alpha_1 = 0.75, \quad \alpha_2 = 0.6, \quad \alpha_3 = 0.3. \quad (4)$$

The average of the smallest plaquette jumps from -0.75 to 1.95. This is about the best that can be achieved with the hypercubic blocking. It is important to remember that we are maximizing the smallest plaquette values on the lattice, not the average plaquettes, which on these lattices are 1.67 and 2.82, respectively. The minimum plaquette is not a well defined physical quantity, it strongly depends on the lattice size, but as long as we compare different actions on the same set of configurations, the minimum plaquette shows how the most severe vacuum fluctuations change during smoothing. In figure 2/b we compare the minimum plaquette distribution of the thin link action to a one-level APE

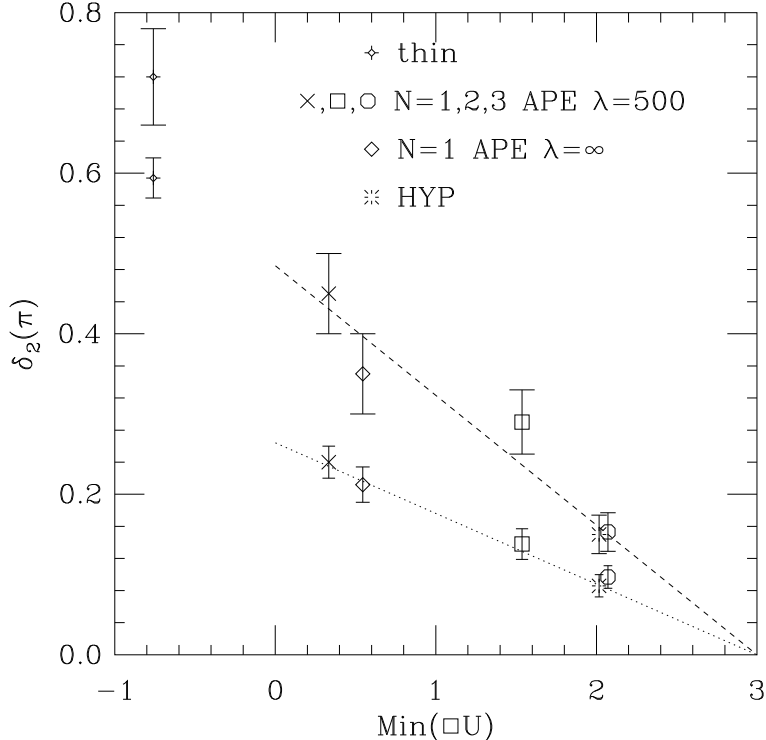


FIG. 3: The parameter δ_2 of eq. (5) for the two lightest non-Goldstone pions $\pi_{i,5}$ (lower points) and $\pi_{i,j}$ (higher points) as the function of the minimum plaquette average of the fat link actions. The pion spectrum is computed on $8^3 \times 24$, $\beta = 5.7$ quenched configurations, the minimum plaquette average on 4^4 , $\beta = 5.7$ configurations. The dotted ($\pi_{i,5}$) and dashed ($\pi_{i,j}$) lines show how the flavor symmetric limit is approached as the minimum plaquette approaches three.

smearing action with $\alpha = 0.7$ on the same configurations that were used to obtain figure 2/a. Here the minimum plaquette average increases only to 0.45 after smearing. Note that it is very important to project to $SU(3)$ the intermediate decorated links in eqs. (1)-(3). Without the projection the resulting hypercubic smearing is not better than a one-level APE transformation.

B. Flavor symmetry Restoration with Fat Link Actions

In the previous section we described an intuitive and fast way to optimize fat link actions by maximizing the minimum plaquette average in finite volume lattices. In this section we show that, as expected, this method optimizes flavor symmetry as well. We compare the level of flavor symmetry restoration of a few fat link actions with their respective minimum

plaquette average computed on 4^4 configurations at $\beta = 5.7$. We use the parameter [4]

$$\delta_2 = \frac{m_\pi^2 - m_G^2}{m_\rho^2 - m_G^2} \quad (5)$$

extrapolated to $m_G/m_\rho = 0.55$ to quantify the difference between the mass of the true Goldstone pion m_G and the mass of the pseudoscalar particles or pions m_π . For a flavor symmetric action $\delta_2 = 0$ for all the pions π . We calculated the meson spectrum on an ensemble of $8^3 \times 24$, $\beta = 5.7$ quenched configurations using the thin link, the N=1, 2, and 3 levels probabilistic APE blocked actions with $\alpha = 0.7$ and projection parameter $\lambda = 500$ (for the definition of probabilistic blocking and the projection parameter see Ref. [6]), the N=1 deterministic ($\lambda = \infty$) APE blocked action and the hypercubic blocked action. Our results are summarized in figure 3 where we plot δ_2 for the two lightest non-Goldstone pions, $\pi_{i,5}$ with flavor structure $\gamma_i\gamma_5$ (lower points) and $\pi_{i,j}$ with flavor structure $\gamma_i\gamma_j$ (higher points) as the function of the minimum plaquette of the fat link actions. δ_2 seems to depend on the minimum plaquette linearly approaching the flavor symmetric limit $\delta_2 = 0$ as the dotted ($\pi_{i,5}$) and dashed ($\pi_{i,j}$) lines in figure 3 indicate, though we do not have a theoretical explanation why this dependence should be linear. The HYP action has about the same flavor symmetry violation than the N=3 APE action that we studied in Ref. [6] reducing δ_2 by about a factor of six relative to the thin link action.

The data in figure 3 are extrapolated to $m_G/m_\rho = 0.55$, a value considerably higher than the physical value 0.175 of this ratio. Since flavor symmetry violation increases as the quark mass decreases, it is important to see how far one can lower the quark mass before flavor symmetry is ruined. In figure 4/a we plot the relative mass splitting

$$\Delta_\pi = \frac{m_\pi - m_G}{m_G} \quad (6)$$

between the lightest non-Goldstone pion $\pi_{i,5}$ and the Goldstone pion G as the function of $(r_0 m_G)^2$ on $\beta = 5.7$ quenched configurations both for the thin and HYP actions. The first three points at the lowest $r_0 m_G$ values for the thin link action are from Ref. [21]. The ratio Δ_π diverges as the quark mass approaches zero but this divergence is much slower for the HYP action. The relative mass splitting for the HYP action grows to about 30% at $r_0 m_G = 0.70$ where the ratio m_G/m_ρ of the Goldstone pion to the rho mass is 0.23(8). At similar values of the m_G/m_ρ ratio the mass splitting with the thin link action is between 130% and 190%.

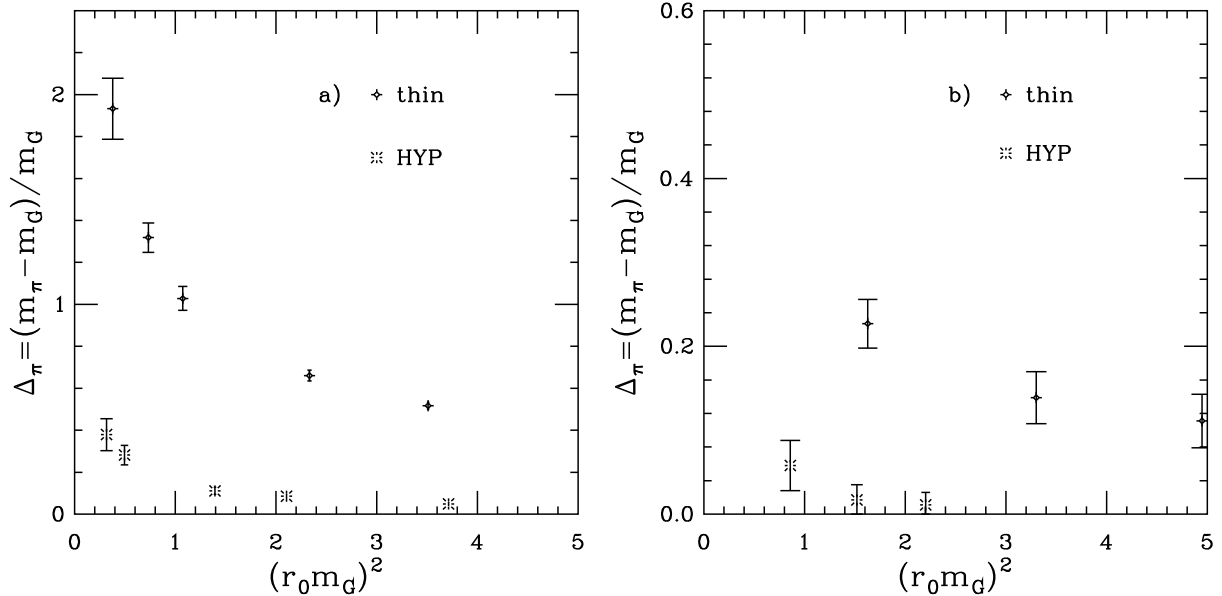


FIG. 4: a) The relative mass splitting Δ_π of eq. (6) between the lightest non-Goldstone pion $\pi_{i,5}$ and the Goldstone pion G as the function of $(r_0 m_G)^2$ on $\beta = 5.7$ quenched configurations both for the thin (fancy diamonds) and the HYP (bursts) actions. b) Same as a) but on $\beta = 6.0$ quenched configurations where the lattice spacing is reduced by about a factor of 2. The first three points at the lowest $r_0 m_G$ values for the thin link action in both figures are from Ref. [21].

C. Hypercubic blocking on Finer Lattices

We have demonstrated that the minimum plaquette value strongly correlates with the level of flavor symmetry restoration at the same lattice spacing. The question naturally arises: if we decrease the lattice spacing, will the smearing be effective or do we have to increase the number of smearing iterations? In figure 5 we show the minimum plaquette value calculated with the thin and hypercubic actions with the optimized parameters of eqn. (4) at $\beta = 5.7, 6.0$ and 6.2 . These calculations were done on 8^4 lattices, that is why the $\beta = 5.7$ result looks significantly worse than before: on a larger lattice the probability of finding a large plaquette fluctuation is higher. The difference between the three β values is striking. One certainly does not need more smearing at a higher coupling. As β increases, the fat link minimum plaquette value increases faster than the corresponding thin link minimum plaquette. That implies that one level of hypercubic blocking will be effective for all coupling values. To verify this expectation we calculated the HYP staggered meson spectrum on a set

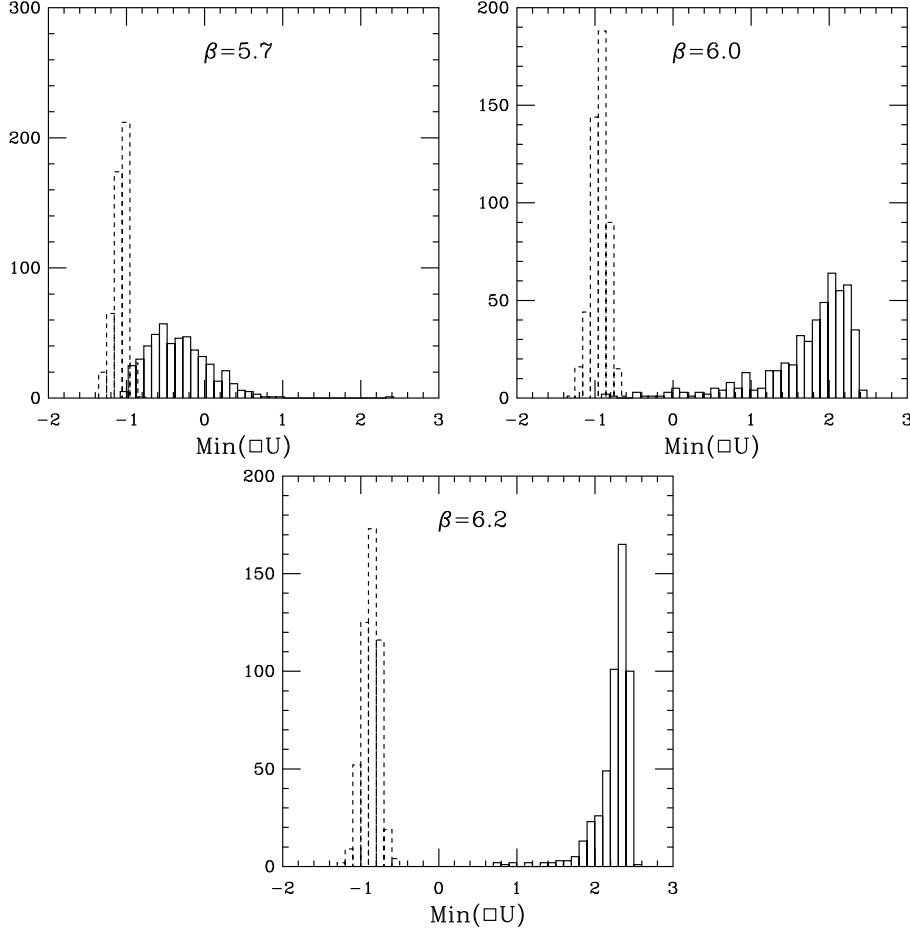


FIG. 5: The histograms of the smallest plaquette distribution on sets of 8^4 gauge configurations at different β values (dashed lines) and after hypercubic blocking (solid lines) on the same configurations.

of $16^3 \times 32$, $\beta = 6.0$ configurations. The configurations were downloaded from the NERSC archive [22]. The mass splitting Δ_π for the lightest non-Goldstone pion $\pi_{i,5}$ is plotted as the function of $(r_0 m_G)^2$ in figure 4/b. The thin link data are from Ref. [21]. The vertical scale of figure 4/b is one fourth of the vertical scale of 4/a but the qualitative features of the two plots are very similar. Δ_π decreases by an order of magnitude from thin to HYP action, fairly independent of the lattice spacing or quark masses.

III. THE STATIC POTENTIAL OF FAT LINK ACTIONS

In the following we consider the static potential, an observable that is quite sensitive to the smearing of the gauge links. We analyzed two sets of lattices. The first set consists 240

$8^3 \times 24$ configurations generated with the Wilson plaquette action at $\beta = 5.7$. The second set is an ensemble of 220 $16^3 \times 32$ lattices from the NERSC archive generated also with Wilson plaquette action at $\beta = 6.0$ [22]. We calculate the static quark potential on both sets using thin links and hypercubic smeared links.

The static potential on pure gauge lattices has been measured and analyzed by several groups on larger lattices with orders of magnitude higher statistics. Our goal here is not the improvement of existing potential measurements, rather we want to demonstrate that the HYP action changes the potential only at small distances, $r/a < 2$ and, due to the smoothness of the gauge configuration, provides an improved signal both for the Sommer parameter r_0 [23] and even more for the string tension. The HYP potential also shows reduced rotational symmetry violation. Our fitted values for r_0/a and $a\sqrt{\sigma}$ are consistent with previously published results.

We extracted the potential by fitting the time dependence of the different Wilson loops to a single exponential. We have measured the on-axis $(m,0,0)$, $m \leq n_x/2$ and three different off-axis sets: $(m,m,0)$, $m \leq n_x/2$, (m,m,m) , $m \leq n_x/2$ and $(m,2m,0)$, $m \leq n_x/4$ (n_x is the number of lattice points in the spatial directions). To reduce statistical errors we used several (20-30) levels of transversal APE smearing on the thin link lattices. After hypercubic blocking the configurations are so smooth that transversal smearing is not important anymore. We used only 5-10 levels of transversal smearing. The statistical errors are from standard jackknife analysis.

In figures 6 and 7 we plot both the thin link and HYP potentials for the $\beta = 5.7$ and $\beta = 6.0$ data sets. The thin link potentials are shifted by a constant value to match the HYP potentials in the $2.5 < r/a < 5.5$ ($\beta = 5.7$) and $2.5 < r/a < 8$ ($\beta = 6.0$) range. Even though the first 5 r/a values were not used for the matching in either coupling, the potentials match closely for $r/a > \sqrt{2}$. The distortion effects in the potential due to smearing are observable only in the first two r/a values, independent of the lattice spacing. Moreover, the HYP potentials have significantly reduced statistical errors, about a factor of 4-7 at $\beta = 5.7$, 10-15 at $\beta = 6.0$. This is most obvious at large distances. For example the $\beta = 6.0$ thin link potential signal becomes extremely noisy for $r/a > 7$ with our statistics while the HYP potential can be easily measured even at the largest distance, $r/a = 11.31$.

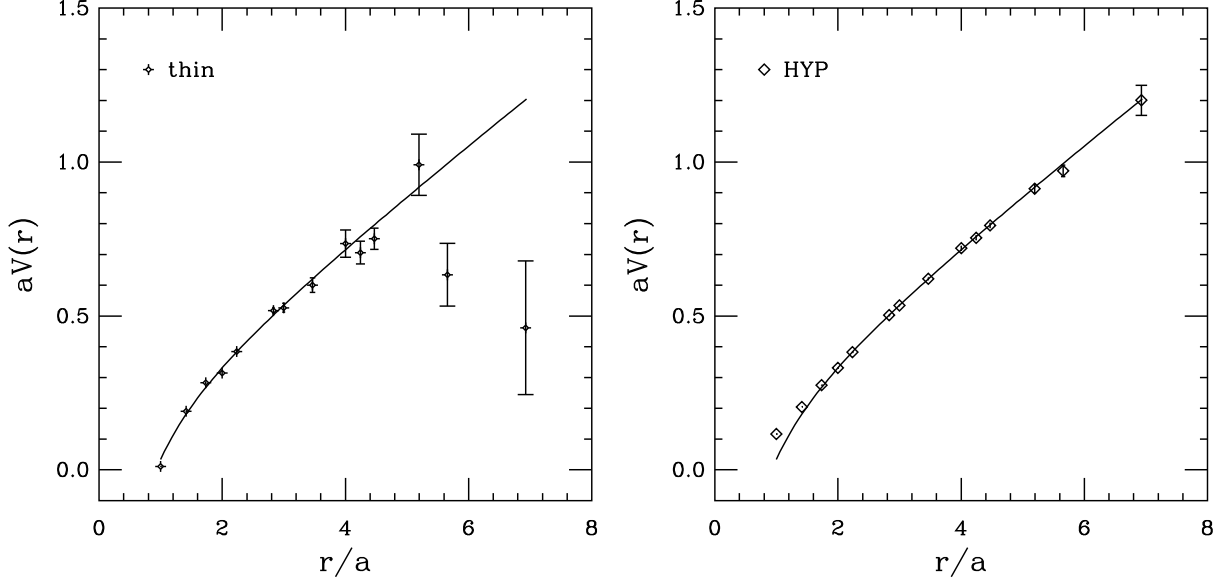


FIG. 6: The thin link and HYP potentials for the $\beta = 5.7$ data set. The thin link potential is shifted by a constant value to match the HYP potential in the $2.5 < r/a < 5.5$ range. The solid line is identical in both plots. It is a three parameter fit of the HYP potential in the range $r/a \in (1.9, 5.5)$.

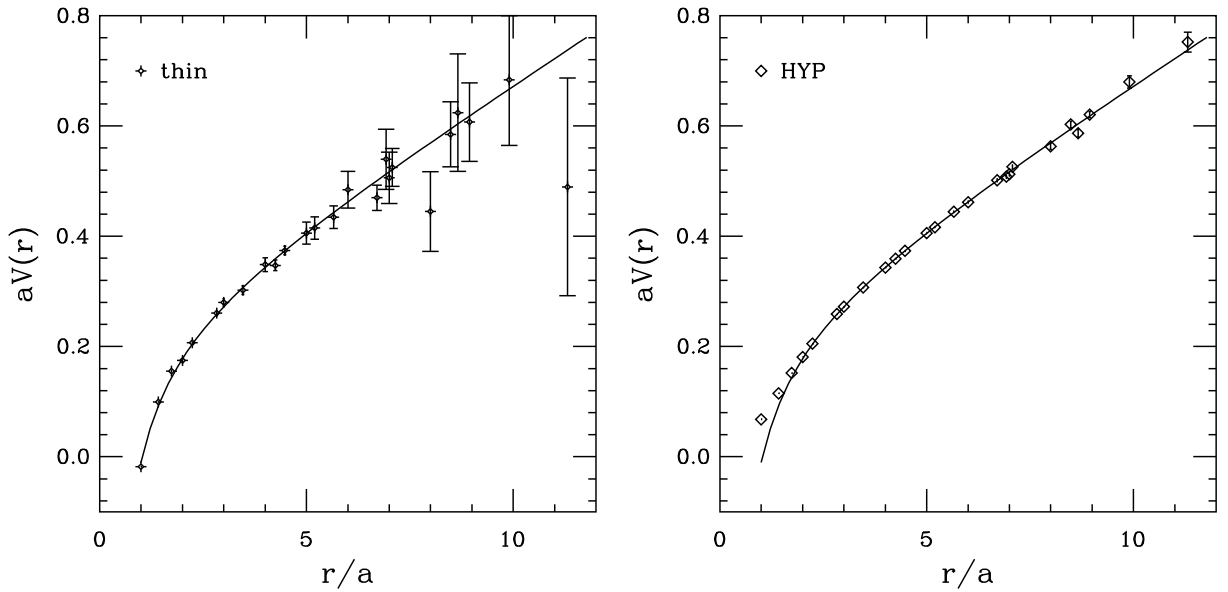


FIG. 7: The thin link and HYP potentials for the $\beta = 6.0$ data set. The thin link potential is shifted by a constant value to match the HYP potential in the $2.5 < r/a < 8$ range. The solid line is identical in both plots. It is a three parameter fit of the HYP potential in the range $r/a \in (2.5, 12)$.

| | r_0/a | $a\sqrt{\sigma}$ | N_{conf} | |
|---------------|-----------|------------------|------------|-----------|
| $\beta = 5.7$ | 2.96(2) | 0.394(7) | 240 | HYP |
| | 2.990(24) | 0.3879(39) | 4000 | Ref. [24] |
| | 2.922(9) | – | 1000 | Ref. [25] |
| $\beta = 6.0$ | 5.36(4) | 0.218(2) | 220 | HYP |
| | 5.369(9) | 0.2189(9) | 4000 | Ref. [24] |

TABLE I: Results obtained with the HYP potential using a global fit of the form of eq. (7). Also included are some large scale simulation results at the same coupling values.

To extract r_0 and $\sqrt{\sigma}$ from our data we fit the potential in the form

$$V(r) = \frac{c_0}{r} + c_1 + c_2 r \quad (7)$$

in a range $r_{min} < r < r_{max}$. r_{max} is limited by the accuracy of our data, $r_{max}/a = 6 - 7$ for the thin link, $10 - 12$ for the HYP potential at $\beta = 6.0$. We choose r_{min} to exclude the region where the potential is changed by the smearing or where short distance lattice artifacts are large, typically $r_{min}/a = 1 - 3$. We do not include any lattice correction in the fit. For one, we do not know the perturbative potential for the HYP action, though it can be calculated. On the other hand we do not seem to need it as the HYP potential data shows only minimal lattice artifacts. Our results obtained with the HYP potentials are summarized in Table I. Fits to our thin link potentials gave consistent results but with much higher statistical errors and are not listed. In Table I we also include results from a few large scale potential simulations with thin links [24, 25]. We considered several r_{max} and r_{min} values and included all on- and off-axis data points in the given range in a global fit to eq. (7). The errors in Table I represent the average jackknife error of the different fits. Our values for r_0/a and $a\sqrt{\sigma}$ from the HYP potential are consistent with the results from large scale computations.

We would like to emphasize that the HYP potential has about an order of magnitude smaller statistical errors than the thin link potential on the same set of configurations. This allowed us to extract the parameters of the potential with precision comparable to the large scale simulations even though our analysis is not as refined. In particular we did not use the one-link integral or multi-hit procedure [26] for the timelike links in the Wilson loops as has been done in [25].

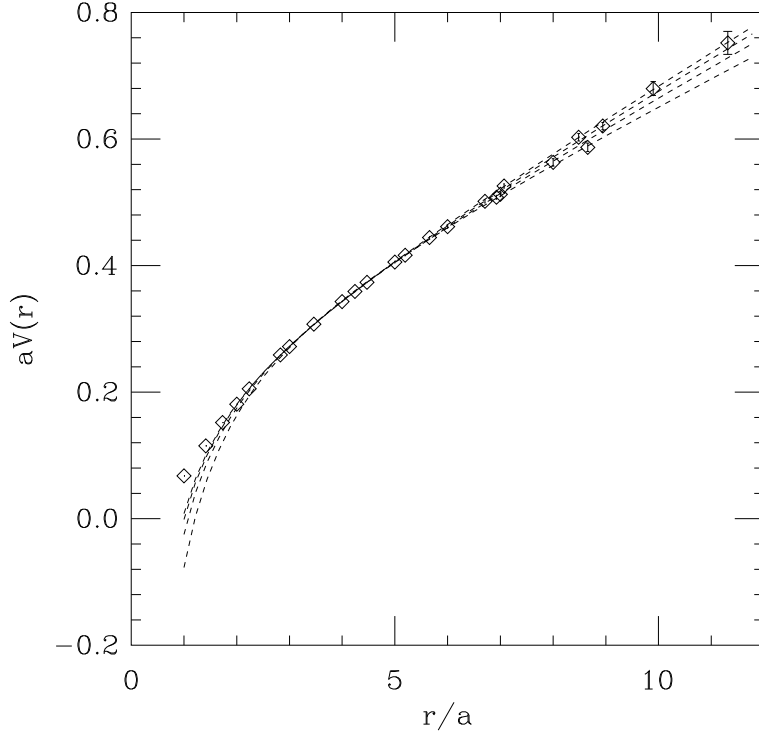


FIG. 8: The HYP potential at $\beta = 6.0$. The dashed lines are fits with eq. (7) along the different on- and off-axis directions the potential is measured. All four fits use the range $r/a \in (2.5, 12)$.

In addition to the reduced statistical errors the HYP potential shows better rotational invariance as well. We use the same quenched configurations both for the thin and HYP potentials, but rotational symmetry violations can come not only from the configurations but also from the operator used to measure the potential. As an example we mention the potential for a perfect action [27]. A perfect action has no scaling violations, yet the perturbatively calculated potential is not rotational invariant unless one uses a perfect potential operator. The HYP operator is of course not perfect, but it appears to be better than the thin link Wilson loop operator. To illustrate rotational symmetry restoration, we separated the on-axis and the three off-axis directions of the $\beta = 6.0$ potential and fitted them independently with the form of eq. (7). The fits for the thin link potential were very poor but for the HYP potential all four fits gave consistent results. We fitted the HYP potential in the range $r/a \in (2.5, 12)$. The fitted values for r_0/a were all within one standard deviation, for $a\sqrt{\sigma}$ within two standard deviations. The fit results are shown in figure 8. The four fitted lines agree very well in the range $r/a \in (2.5, 6.5)$, they deviate at larger r/a due to the slightly different $a\sqrt{\sigma}$ values. The uncertainty of the fitted lines is comparable to their

spread in figure 8. Closer inspection of the data points reveals some rotational symmetry violation even with the HYP potential. It should be possible to correct for some of these effects perturbatively thereby increasing the accuracy of the scale determination.

The improved rotational symmetry of the HYP potential is not the main motivation for using the HYP operator to measure the potential. Improved gauge actions can be even more effective in restoring rotational invariance of the static potential [28, 29, 30]. The improvement of statistical accuracy by an order of magnitude of the HYP potential as compared to the thin link potential is a more important feature.

IV. SUMMARY

In this paper we introduced a new kind of fat link, the hypercubic (HYP) fat link. The HYP fat link is constructed to be localized, it does not extend beyond hypercubes attached to the original link. The construction has three free parameters that are optimized to reduce large plaquette fluctuations.

Using quenched configurations at $\beta = 5.7$ and $\beta = 6.0$ we calculated the staggered spectrum of the HYP action. We showed that at both coupling values flavor symmetry is greatly improved. The relative mass splitting, $\Delta_\pi = (m_G - m_\pi)/m_G$ is reduced by an order of magnitude at fixed $r_0 m_G$, independent of the coupling and the quark mass as well.

We have also considered the static potential calculated on HYP smeared $\beta = 5.7$ and $\beta = 6.0$ configurations. We showed that smearing changes the potential only at distances $r/a < 2$ yet reduces statistical errors by about an order of magnitude. Even with the very limited statistics of 220-240 lattices we could extract both the Sommer parameter r_0/a and the string tension $a\sqrt{\sigma}$. Our results for both of these quantities are consistent with large scale simulation results with errors that are better than our statistics would indicate from the thin link potential.

We have undertaken this quenched study on the properties of the hypercubic blocking because we want to do dynamical simulations with the HYP action. Such simulations are feasible using combined over-relaxation and heat-bath updates. In a forthcoming publication [19] we use the dynamical HYP action in a finite temperature simulation to show how improved flavor symmetry changes the phase diagram of four-flavor dynamical staggered fermions.

V. ACKNOWLEDGEMENTS

We are grateful to Prof. T. DeGrand for many useful discussions during the course of this work. This work was supported by the U.S. Department of Energy. We thank the MILC collaboration for the use of their computer code.

-
- [1] T. Blum et al., Phys. Rev. **D55**, 1133 (1997), hep-lat/9609036.
 - [2] J. F. Lagae and D. K. Sinclair, Phys. Rev. **D59**, 014511 (1999), hep-lat/9806014.
 - [3] K. Orginos, D. Toussaint, and R. L. Sugar (MILC), Phys. Rev. **D60**, 054503 (1999), hep-lat/9903032.
 - [4] K. Orginos and D. Toussaint (MILC), Phys. Rev. **D59**, 014501 (1999), hep-lat/9805009.
 - [5] F. Karsch, E. Laermann, and A. Peikert, Phys. Lett. **B478**, 447 (2000), hep-lat/0002003.
 - [6] F. Knechtli and A. Hasenfratz (2000), hep-lat/0012022, accepted for publication in Phys. Rev. D.
 - [7] T. DeGrand, A. Hasenfratz, and T. G. Kovacs, Nucl. Phys. **B547**, 259 (1999), hep-lat/9810061.
 - [8] M. Stephenson, C. DeTar, T. DeGrand, and A. Hasenfratz, Phys. Rev. **D63**, 034501 (2001), hep-lat/9910023.
 - [9] W. Bietenholz (2000), hep-lat/0007017.
 - [10] T. DeGrand (MILC), Phys. Rev. **D63**, 034503 (2001), hep-lat/0007046.
 - [11] T. DeGrand and A. Hasenfratz (2000), hep-lat/0012021.
 - [12] W. Bardeen, A. Duncan, E. Eichten, G. Hockney, and H. Thacker, Phys. Rev. **D57**, 1633 (1998), hep-lat/9705008.
 - [13] W. Bardeen, A. Duncan, E. Eichten, and H. Thacker, Phys. Rev. **D57**, 3890 (1998).
 - [14] T. DeGrand, A. Hasenfratz, and T. G. Kovacs, Nucl. Phys. **B520**, 301 (1998), hep-lat/9711032.
 - [15] A. Hasenfratz and C. Nieter, Phys. Lett. **B439**, 366 (1998), hep-lat/9806026.
 - [16] C. Bernard, Nucl. Phys. Proc. Suppl. **94**, 159 (2001), hep-lat/0011064.
 - [17] C. Bernard et al., Nucl. Phys. Proc. Suppl. **94**, 346 (2001), hep-lat/0011029.
 - [18] T. DeGrand (2001), private communication.
 - [19] A. Hasenfratz and F. Knechtli (2001), in preparation.
 - [20] M. Albanese et al. (APE), Phys. Lett. **B192**, 163 (1987).

- [21] R. Gupta, G. Guralnik, G. W. Kilcup, and S. R. Sharpe, *Phys. Rev.* **D43**, 2003 (1991).
- [22] G. Kilcup, D. Pekurovsky, and L. Venkataraman, *Nucl. Phys. Proc. Suppl.* **53**, 345 (1997), hep-lat/9609006.
- [23] R. Sommer, *Nucl. Phys.* **B411**, 839 (1994), hep-lat/9310022.
- [24] R. G. Edwards, U. M. Heller, and T. R. Klassen, *Nucl. Phys.* **B517**, 377 (1998), hep-lat/9711003.
- [25] M. Guagnelli, R. Sommer, and H. Wittig (ALPHA), *Nucl. Phys.* **B535**, 389 (1998), hep-lat/9806005.
- [26] G. Parisi, R. Petronzio, and F. Rapuano, *Phys. Lett.* **B128**, 418 (1983).
- [27] T. DeGrand, A. Hasenfratz, P. Hasenfratz, and F. Niedermayer, *Nucl. Phys.* **B454**, 587 (1995), hep-lat/9506030.
- [28] T. DeGrand, A. Hasenfratz, P. Hasenfratz, and F. Niedermayer, *Nucl. Phys.* **B454**, 615 (1995), hep-lat/9506031.
- [29] G. P. Lepage, *Nucl. Phys. Proc. Suppl.* **47**, 3 (1996), hep-lat/9510049.
- [30] Y. Iwasaki, K. Kanaya, T. Kaneko, and T. Yoshie, *Phys. Rev.* **D56**, 151 (1997), hep-lat/9610023.